

Multiscale Modeling of a Nanoelectromechanical Shuttle

C. Huldt* and J.M. Kinaret

Department of Applied Physics, Chalmers University of Technology, S-412 96 Göteborg, Sweden

(Dated: December 29, 2021)

In this article, we report a theoretical analysis of a nanoelectromechanical shuttle based on a multiscale model that combines microscopic electronic structure data with macroscopic dynamics. The microscopic part utilizes a (static) density functional description to obtain the energy levels and orbitals of the shuttling particle together with the forces acting on the particle. The macroscopic part combines stochastic charge dynamics that incorporates the microscopically evaluated tunneling rates with a Newtonian dynamics.

We have applied the multiscale model to describe the shuttling of a single copper atom between two gold-like jellium electrodes. We find that energy spectrum and particle surface interaction greatly influence shuttling dynamics; in the specific example that we studied the shuttling is found to involve only charge states $Q = 0$ and $Q = +e$. The system is found to exhibit two quasi-stable shuttling modes, a fundamental one and an excited one with a larger amplitude of mechanical motion, with random transitions between them.

I. INTRODUCTION

Nanoelectromechanical systems that combine electrical and mechanical functionalities on the nanometer scale have in the recent years attracted a great deal of theoretical and experimental interest.^{1,2} The nanoelectromechanical shuttle is a structure that resembles a single electron transistor but incorporates mechanical motion of the central island. Previous theoretical works on the shuttle have shown that in the presence of an DC applied bias the charge and velocity of the central island are correlated, $Q(t)\dot{Z}(t) \neq 0$, which implies that the shuttle absorbs energy from the DC field and converts it into mechanical motion. The shuttle motion facilitates charge transfer through the system, and signatures of mechanical motion can be seen both in the current-voltage characteristics and in the noise properties of the device.^{3,4,5}

Several theoretical studies have been carried out for different setups of the shuttle since the first description of this phenomenon. The theoretical studies cover different size regimes of the shuttle, featuring coherent⁶ or sequential^{7,8} tunneling and quantum mechanically^{9,10} or classically^{11,12} described mechanical motion. The studies have shown that the shuttle instability strongly depends on the bias voltage and the system setup. This sensitivity also renders the shuttle behavior dependent on the precise description of the problem.

Experimental evidence of coupling between vibrational degrees of freedom and electron transfer has been found for both microscopic^{13,14} and macroscopic¹⁵ systems. In particular, the experiment by Park *et al.*, reference 16, using a C₆₀ molecule between gold electrodes has demonstrated the type of coupling that has been considered by many theoretical studies and has increased the interest for a molecular shuttle.^{6,9,10,12,17}

In the shuttle geometry the mechanical motion is on a nearly macroscopic time scale, typically from picoseconds for small molecules to nanoseconds for large molecules such as carbon nanotubes. The motion is excited due to tunneling events between the mobile object and the sta-

tionary electrodes, which have a typical timescale of femtoseconds and are determined by the electronic structures of the mobile molecule and the electrodes. Hence, a theoretical description of the shuttle system naturally calls for multiscale methods that combine the fast electronic time scales with the slower mechanical ones. Thus far research has concentrated on the slow degrees of freedom while dealing with the fast ones in a phenomenological approximation.

The two main issues addressed in this work are the impact of the electronic structure of the central island on the shuttling motion, and an analysis of the short range interactions between the central island and the stationary electrodes. The first issue we will address by describing the central island using density functional theory,^{18,19} which provides information on the energy spectrum of the island as well as structure of the relevant orbitals. The interaction between the island and the electrodes is described in part by a phenomenological Born-Mayer potential combined with image charge effects, and in part by a model that transfers mechanical energy from the shuttle to lattice vibrations in the electrodes, thereby dissipating energy of the shuttle system and preventing catastrophic runaway. Due to the phenomenological description of surface interactions, some physical effects such as chemisorption are not properly accounted for which limits the applicability of the present model to materials for which chemisorption can be neglected. A way to overcome this problem in a future study would be to incorporate a time-dependent DFT²⁰ module that describes both the island and the electrode during the crucial parts of the shuttle cycle; at present, however, that type of description is prohibitively expensive from a computational point of view.

The DFT data is used to evaluate tunneling matrix elements and tunneling rates between the central island and the electrodes. These are then inserted to a dynamic module that describes both the charge dynamics in terms of stochastic tunneling events and mechanical motion using molecular dynamics. The resulting macroscopic dy-

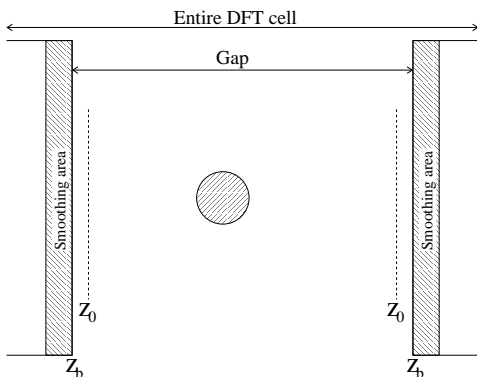


FIG. 1: The system. A copper atom is placed in between two jellium surfaces 15 Å apart. A buffer with the width of 2.5 Å is added on both side of the gap for the DFT calculations in order to localize the electrons. A small smoothing area between gap and barrier is needed to speed up calculations.

namics is implemented as a dynamic Monte Carlo algorithm that uses the output of a series of static DFT calculations as its input. This stochastic dynamics can be used to address both average transport properties such as current and random fluctuations, or noise, which both exhibit clear signatures of shuttling according to phenomenological theories.

II. METHOD

A. Setup

For computational efficiency, we have chosen to focus on the simplest possible system where the central island comprises just one atom. However, the methods and qualitative results should be applicable also to more complex system. The system we consider includes two electrodes 15 Å apart, described as semi-infinite jellium slabs. The central island is a copper atom that can move in a direction normal to the electrode surfaces. For the electrodes, the Wigner-Seitz radius is set to 3 a.u. and the electrode work function W is set to 3.5 eV.²¹ The fermi energy, ϵ_F , is calculated from the Wigner-Seitz radius while other material specific electrode parameters are taken from gold. A bias voltage of 3 V is applied over the gap, the potential dropping from left to right. The region described by the DFT module consists of the region between the two electrodes plus a buffer region of 2.5 Å inside each of the electrodes as show in Fig. 1. The buffer regions are needed so that the plane-wave-based code can better describe orbitals that are localized in the inter-electrode gap.

B. Electronic structure calculations

The electrodes and the space between them are treated separately: the electronic structure of the shuttling object is described using a density functional code that is limited to the inter-electrode space while the electrodes themselves are described analytically within the jellium approximation. For the electronic structure calculation we use the DaCapo code²² with the PW91 exchange correlation functional²³ and employ the adiabatic approximation to separate the electronic structure calculation from the dynamics description.

The effect of the electrodes on the island is modeled as a one-electron potential and inserted directly into the effective potential in the Kohn-Sham equations. The potential is divided into two parts: the interaction between an electron and a metal surface, and the interaction between an electron and the induced charge arising from the remaining charges in the space between the electrodes. For the former part we use the saturated image barrier

$$V_J(z) = \begin{cases} -\frac{q^2}{16\pi\epsilon_0(z-z_0)}(1-e^{-\lambda(z-z_0)}) & z \geq z_0 \\ -\frac{V_0}{Ae^{B(z-z_0)}+1} & z \leq z_0, \end{cases} \quad (1)$$

suggested by Jones and Jennings.²⁴ Here the parameters are related to the work function W and Fermi energy ϵ_F of the electrodes through $V_0 = W + \epsilon_F$, $A = -1 + 16\pi\epsilon_0 V_0/q^2\lambda$ and $B = 8\pi\epsilon_0 V_0/q^2 A$ where the parameters z_0 and λ are found by fitting eq. (1) with DFT calculated tabulated data on the effective potential, v_{eff} .²⁵ The values were determined to $\lambda = 1.6 \text{ \AA}^{-1}$ and $z_0 = 0.34 \text{ \AA}$ outside the jellium background z_b . The suppression factor $(1 - \exp(-\lambda(z - z_0)))$, which multiplies the classical image potential, tends towards zero as the mirrored charge closes in on the surface. The image plane, z_0 , is used as the effective surface of the material, in compliance with Lang and Kohn.²⁶ The value of z_0 derived for eq. (1) differs from the value derived by Lang and Kohn for *e.g.* image charge potential.²⁷ However, for the interactions with the induced charge, the individual contributions from the electrons and the nucleus should cancel out far from the surface and it is therefore suitable to keep only one parameter for the effective surface.

For the second term, the potential at \mathbf{r} due to a charge at position \mathbf{r}' , we use a form $v(\mathbf{r}; \mathbf{r}')$ that satisfies Poisson's equation in the region outside the electrodes and reduces to the saturated image potential if the mirrored charge is at the same point where the potential is measured giving

$$v(\mathbf{r}; \mathbf{r}') = -\frac{q^2}{4\pi\epsilon_0 |\mathbf{r} - \tilde{\mathbf{r}}'|} \left(1 - e^{-\lambda(z' - z_0)}\right) \quad (2)$$

The resulting potential for interaction with the core is

$$V_{In}(\mathbf{r}) = Q_v v(\mathbf{r}; \mathbf{Z}), \quad (3)$$

where Q_v is the core charge of the island, *i.e.*, the number of protons minus the number of core electrons.

The model for the interaction with the induced charge from the other electrons is obtained similarly. Here we assume that the electron distribution of the island is well approximated with a Gaussian, as is typically the case, and integrate over the mirrored charge to obtain

$$V_{Ie}(\mathbf{r}) = -(Q_e - 1) \int d\mathbf{r}' v(\mathbf{r}; \mathbf{r}') \rho(\mathbf{r}'). \quad (4)$$

where

$$\rho(\mathbf{r}') = \frac{1}{(2\pi)^{3/2} \sigma^3} e^{-\frac{1}{2}(\mathbf{Z}-\mathbf{r}')^2/\sigma^2} \quad (5)$$

is a form function and Q_e is the number of valence electrons for the central island. The width $\sigma(Q)$ is calculated by fitting a Gaussian to the unperturbed electron density for different charge states, Q denoting the number of extra charge units on the central island. Assuming localization of electrons to the island or the leads (no chemisorption), Q is strictly integer.

The added bias voltage is

$$V_{bias}(z) = E(z - \Delta_{gap}/2) \quad (6)$$

where the electric field is $E = V/(\Delta_{gap})$ and Δ_{gap} the distance between the electrodes. Finally, the Pauli repulsion that confines electrons within the gap is for the electronic structure calculations described as a repulsive square potential wall placed at z_b . The repulsion term is important for the separation of electronic structure calculation and charge transfer mediated by tunneling, however, the form of the repulsion is less important as most of the tunneling events take place when the island is relatively far from the surface on an atomic scale.

Owing to the time-consuming and time-independent character of DFT, it is not possible to determine the system properties continuously. Instead, the simulations are performed on a number of positions and charge states. A continuous description is produced with interpolation.

C. Forces

The forces on the atomic core are calculated using the DFT code. In the Kohn-Sham single-particle equations all charges but one electron are treated as a mean-field static charge distribution. We implement the potential due to surface interactions as an external field. This results in proper (mean field) orbitals and energy eigenvalues but incorrect forces and total energies. Therefore, a correction term in the form of $\frac{\partial V_{DFT}}{\partial Z} - \frac{\partial V_{el}}{\partial Z}$ is added to the forces calculated by the electronic structure code. Here, V_{DFT} is the induced charge potential used in the DFT calculation, the sum of eq. (1), (3) and (4). The actual potential, V_{el} is obtained as a variational derivative

of the full electronic energy as

$$V_{el} = \frac{Q_e}{2} \int d^3\mathbf{r}' [v(\mathbf{Z}; \mathbf{r}') + v(\mathbf{r}'; \mathbf{Z})] \rho(\mathbf{r}') - Q_v v(\mathbf{Z}; \mathbf{Z}) + g(\mathbf{r}) \quad (7)$$

where the last term $g(\mathbf{r})$ is independent of Z and does not contribute to the forces.

A smooth many-body short-range repulsion is added to the total force. We have chosen a Born-Mayer type pair potential²⁸ and integrated over the electrode surface which yields the force

$$F(z) = f_0 e^{(\sigma_{Au} + \sigma_{Cu})/\rho} \left(e^{z/\rho} + 2\pi z \rho n_s e^{(-\sqrt{z^2 + a^2}/(2\pi))/\rho} \right). \quad (8)$$

For a Cu-atom outside a gold surface, the effective radii are $\sigma_{Cu} = 0.77$ Å and $\sigma_{Au} = 1.37$ Å, $n_s = 2/a^2$ is the surface density of atoms and $a_{lat} = 4.078$ Å is the lattice constant for a fcc [100] gold surface.^{29,30} The closest electrode lattice site is considered separately (in order to maximize the localization) while the other lattice sites are handled as a continuum. The values f_0 and ρ are $6.95 \cdot 10^{-11}$ N and 0.3 Å respectively.^{31,32,33,34}

D. Transition rates

Charge transfer rates between the central island and electrodes are calculated with the transfer Hamiltonian method^{35,36} using the overlap between the atomic and electrode wave functions. The transition rates to and from a specific atomic orbital are

$$\Gamma_{\rightarrow p} = \frac{V n_f}{(2\pi)^3} \int d^3k \frac{2\pi}{\hbar} |M_{pq}|^2 \delta \left(-W_{R/L} + \frac{\hbar^2 k^2}{2m} - E_p \right) \quad (9)$$

where

$$M_{pq} = \int_{z \in R_{gap}} d^3r \psi_{p,a}^* (V_a - V_m) \psi_{q,m}. \quad (10)$$

Here, $\psi_{p,a}$ is a Kohn-Sham orbital (localized on the island) with eigenenergy E_p , $\psi_{q,m}$ is a metal wave function and n_f is the relevant number of states available for tunneling in the (often degenerate) orbital $\psi_{p,a}$. The potentials V_a and V_m are the effective potentials for $\psi_{p,a}$ and $\psi_{q,m}$ respectively. The atomic orbital $\psi_{p,a}$ and the effective gap potential V_a are extracted from the DFT simulations. The transition rates are calculated numerically for all energetically allowed transitions determined by comparing the electrode chemical potentials with the Kohn-Sham eigenvalues.

The electrode wave functions are calculated analytically from a square potential with a finite barrier at the electrode surface and a hard wall at $-\infty$. The electrode

wave functions in the z -direction are

$$\psi_{k_z}(z) = \begin{cases} \sqrt{\frac{2\kappa_z}{\kappa_z L + 1}} \sin \delta_z e^{-\kappa_z z} & z \geq 0 \\ \sqrt{\frac{2\kappa_z}{\kappa_z L + 1}} \sin(k_z z - \delta_z) & -L \geq z \geq 0 \end{cases} \quad (11)$$

with $\kappa_z = \sqrt{\frac{2mW}{\hbar^2} - k_z^2}$ and $\delta_z = \arcsin(\frac{\hbar k_z}{\sqrt{2mW}})$. A small offset between the physical and the geometrical surface is implemented to attain charge neutrality of the jellium slabs.²¹ Periodic boundary conditions are assumed parallel to the surface.

E. Dynamics

A dynamic Monte Carlo approach is used to calculate the shuttle dynamics. Input parameters to this module consist of core forces and transition rates as functions of the island position. The motion of the central island is described classically by

$$m\ddot{x} = F_{ext}(x, Q) + F_{dissip}(x, Q) \quad (12)$$

where F_{ext} are the core forces given by the previous calculations and F_{dissip} is a dissipation term. The island position $x(t)$ is calculated by numerically integrating the equation of motion, while the island charge $Q(t)$ is allowed to change stochastically using the tunnel rates determined above. This results in a coupled stochastic dynamics for the mechanical and electrical degrees of freedom.

As the shuttle absorbs energy from the bias voltage, the dissipation term is essential for the stability of the island motion.^{3,37} Earlier theoretical work has mainly used viscous damping, $-\eta\dot{x}$.^{3,12,38,39,40} In this work a different model based on mechanical damping is used, coupling a simple model of the surface to the island equation of motion via the surface forces as

$$\begin{cases} m\ddot{x} = F_{tot}(x) - X F'_{tot}(x) \Theta(X F'_{tot}(x) \dot{x}) \\ M\ddot{X} = -M\dot{X} - kX - F_{tot}(x - X), \end{cases} \quad (13)$$

where x and m are the position and mass of the central island, X and M are the position and mass of the surface, and k is an effective surface spring constant. The Θ -function in the first equation restricts the energy flow so that the shuttle energy can be transferred to lattice vibrations of the electrodes (phonon emission) while the opposite process of phonon absorption is forbidden.

The equations have been formulated in terms of the surface element nearest to the shuttling object, which implies that the effective mass of the surface depends on the separation between the mobile island and the surface; this can be determined by assuming an elastic model for the surface and requiring that (i) the instantaneous displacement $X(t)$ agrees with that of the surface atom nearest to the shuttling object, and (ii) the total momentum of the surface is $M\dot{X}$. The elastic parameters for

surface atoms have been chosen to correspond to those of gold, and effective parameters in the simplified model are consequently $M(X) = m_{Au}F(X)/F_{max}(X)$, where $F(X)$ is the total force between the shuttling object and the surface and $F_{max}(X)$ is the force on the surface atom nearest to the shuttle and $k = k_{Au}F(X)/F_{max}(X)$ where $k_{Au} = 8m_{Au}v_s^2/a^2$ is the spring constant obtained from the sound velocity v_s and lattice constant a .

The main qualitative difference between our dissipation model and viscous damping is that in our model dissipation occurs primarily when the island-electrode interaction is strongest. This influences the threshold voltage for onset of shuttling, and also renders the threshold dependent on the initial conditions.

III. RESULTS

The different parts of the one-electron potential are depicted in Fig. (2). The small widths of the form function ($\sigma \sim 0.24$ - 0.27 Å for an unperturbed pseudopotential, $Q = 1 \dots -1$, and ~ 0.30 - 0.35 Å for the double junction potential) imply that sufficiently far from the surface the point charge approximation would be quite accurate: for distances ≥ 2 Å from the surface, the spatial distribution of charge has little effect on the potential. For island positions close to the electrode surfaces, the spread in the valence electron distribution and the rapid saturation effectively bares the core image making the effective potential strongly repellent.

The resulting Kohn-Sham eigenvalues, depicted in Fig. 3, are used as energy spectra for the central island. Comparison between the eigenvalues and the electrode chemical potentials gives the possible transitions. Full relaxation into the $N/2$ lowest bands is assumed instantaneous, where N is the number of valence electrons (11 for the used Cu GGA pseudopotential, $Q = 0$). Higher bands are treated as excitations.⁴¹ The temperature is taken to be zero in the treatment of tunneling events; however, in the DFT calculation a finite temperature is needed for convergence.

A small correction is needed for some calculations in order to use the equilibrium DFT calculations within a dynamic picture. For some island positions and $Q \leq 0$, it is energetically favorable to place some of the extra charge in the surface potential well outside the positive electrode surface instead of on the central island. However, the time scale for this direct equilibration between leads is very long. In order to find the energy spectra and orbitals that are relevant for the dynamic evolution, the surface well near the left electrode surface is manually suppressed for core positions near the right electrode; due to the polarity of the applied bias, similar problems do not arise for core positions near the left electrode. The possibility of transitions directly between the electrodes is kept, but the transition rates are small enough to be of no importance for the results.

For the tunneling rate calculation the Kohn-Sham

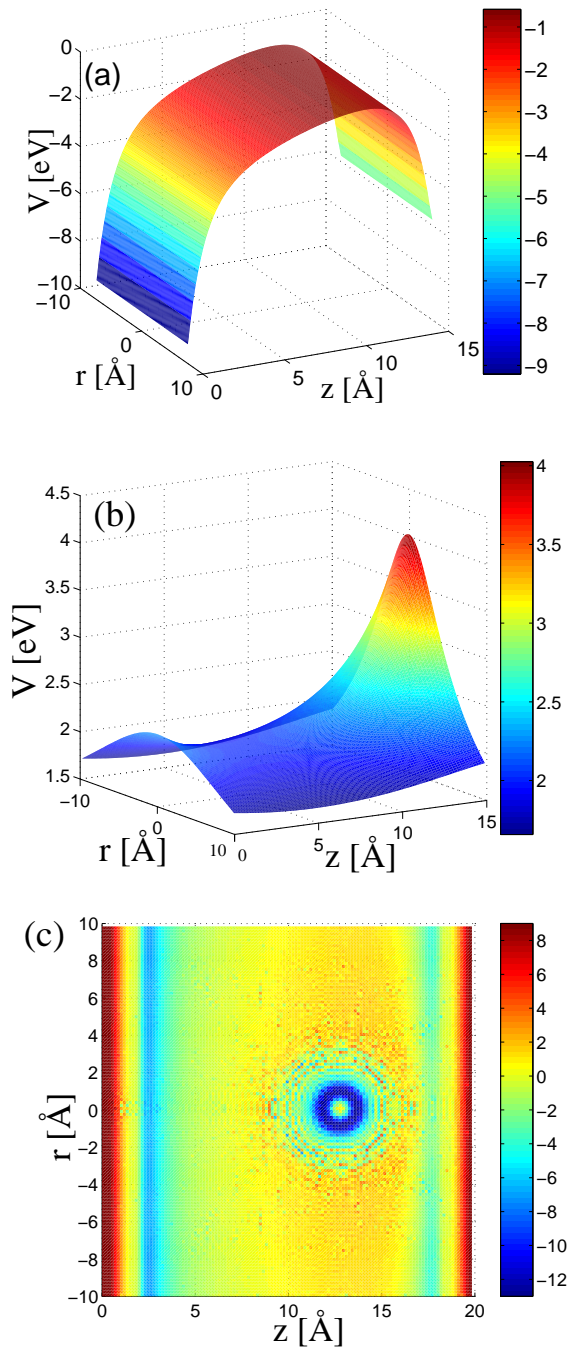


FIG. 2: The Kohn-Sham one-electron effective potential comprises several parts rendering diverse behaviors for different positions and charge states. The above figures are for $Q = 0$ and $Z = 10.17 \text{ \AA}$. The z -axis is the direction of island motion, r is parallel to the electrodes. In (a) and (b) z encompasses the gap while (c) includes the entire DFT cell with the 2.5 \AA buffer regions on both sides of the gap. (a) Equation (1) and the bias voltage. (b) One electron interaction with induced charge due to other system charges. (c) The effective potential as used by DaCapo. Close to the electrodes eq. (1) forms deep wells.

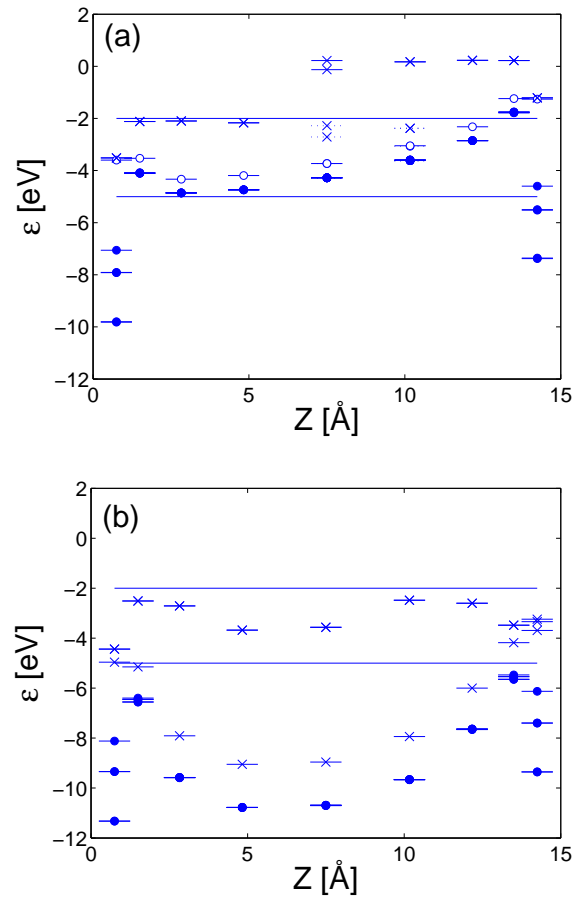


FIG. 3: The lowest eight non-spin polarized Kohn-Sham eigenvalues for nine positions of the central island. Levels indicated by filled circles are fully occupied, empty circles half-occupied and crosses unoccupied. The upper and lower solid lines are μ_R and μ_L respectively. (a) $Q = 0$. The lower lying excitations (core positions in the left half of the gap) have been calculated including the surface potential well near the electrode. The higher lying excitations (core positions near right electrode) have been calculated without the surface potential well near the left electrode as transitions directly from the right electrode to the left surface well have very small tunneling rates. For $Z = 7.5 \text{ \AA}$ and $Z = 10.17 \text{ \AA}$ results are depicted for both approaches (solid and dashed lines). For the positions closest to the electrodes, the width of the surface potential wells causes a substantial drop in eigenenergies. (b) $Q = 1$.

eigenvalues are regarded as electron energies, which is known to be rigorously correct for the ionization potential involving the HOMO level,⁴¹ and believed to be reasonably accurate for the other levels as well.⁴² We assume that tunneling rates are sufficiently low so that the island fully relaxes between each tunneling event to the configuration determined by time-independent DFT. The time scale for this relaxation is typically in the femtosecond range which is fast compared to the tunneling rates except for core positions very close to the electrode sur-

faces; however, since energetics severely limits the possible tunneling processes, the instantaneous relaxation approximation is reasonably well justified for all core positions. For the chosen bias voltage, the possible charge transitions for the island are $1 \rightarrow 0$ and $0 \rightarrow 1$.

It is interesting to notice the asymmetry of attainable charge states that arises from the asymmetry of the energy spectrum of the Cu atom: the dynamical evolution only involves charge states $Q = 0$ and $Q = 1$ but not $Q = -1$. The symmetric expression for charging energy $E = Q^2/2C$ used for larger metallic grains is only justified if the level spacing on the island is small enough so that the electrostatic energy scales dominate. This asymmetry implies that the shuttling is asymmetric also in the sense that energy is absorbed from the DC field only during half a period which makes the system more sensitive to dissipative mechanisms.

The occupied Kohn-Sham eigenfunctions are identified as d - and s -orbitals in accordance with the expected electron configuration of Cu, $3d^{10}4s^1$. Close to the electrode surfaces, the orbitals deform against the repulsion wall. For all but the closest position to the electrodes the $4s$ -orbital gives the widest electron distribution and the largest contribution to the transition rates.

The core forces for the central positions are strongly dependent on the delocalization of the electron distribution of the central island (Fig. 4). For the positive ion with $Q = 1$ the dominant force is the electrical bias while the potential of $Q = -1$ is a nearly symmetric image charge potential. For $Q = 0$, the sign depends on the description of the surface interactions, and with the interaction model we have chosen the neutral atom feels a slight net force towards the negatively charged right electrode. The repulsion from the surface is dominant for the two outermost positions on either side giving a physisorption minimum between 3–5 Å from the electrode surface.

The transition rates are much less sensitive to the surface description than the forces (Fig. 5). Their distance dependence is approximately exponential as assumed by effective theories⁴³ with slight saturation for core positions nearest to the electrodes with a tunneling length that is approximately 0.4 Å with some variation for the different allowed transitions. Near the electrodes the energetics considerations inhibit tunneling, as seen in Fig. 3, which can be viewed as a molecular equivalent of Coulomb blockade.

In the dynamics simulations, the calculated forces and transition rates are joined. The result is indeed a stable shuttling regime where $\dot{Q}(t)\dot{Z}(t) \neq 0$. We have performed dynamical simulations starting from a variety of initial states, and seen that for most starting conditions the results are quite similar: as a rule, the model does indeed shuttle electrons (Fig. 6). However, for some initial configurations such as $Z(t=0) \approx 10$ Å and $Q(t=0) = 0$ the applied bias of 3 V is not sufficient to initiate shuttling. One of the more prominent differences between our results and previous works is the complexity of the forces,

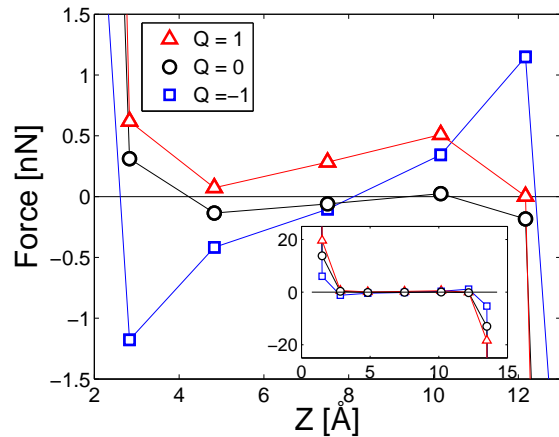


FIG. 4: Total forces on the grain core, center positions. Positions not included $Z = 0.75$ Å and $Z = 14.25$ Å reach $\pm(500 - 650)$ nN. Lines between positions correspond to the used interpolation scheme.

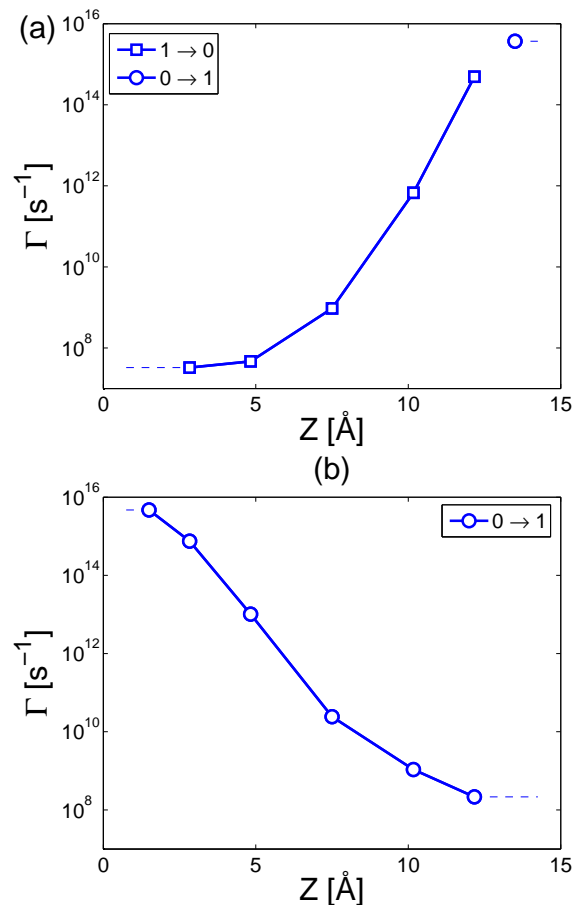


FIG. 5: Transition rates: electron current from right to left. (a) Squares: Transitions from negative right lead to island. Close to the negative lead, current mediating transfer is blocked by energetics (Coulomb blockade). Instead, an electron can transfer against the bias back to the negative lead, (circles). (b) Electron transitions from island to positive left lead.

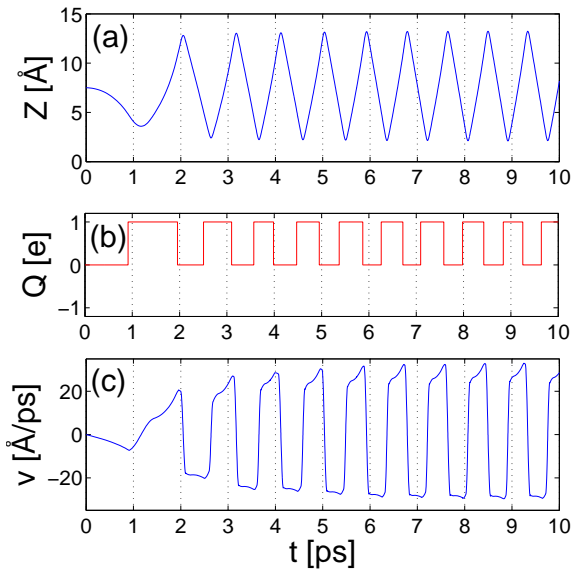


FIG. 6: Shuttle regime for initial conditions $Z(0) = 0$, $Q(0) = 0$ and $v(0) = 0$. (a) Island position. (b) Charge state as a function of time. The shuttle carries one electron per period. (c) Island velocity. The main acceleration and deceleration are close to the electrodes.

particularly near the electrode surfaces. Since the surface description we use is adapted from static analyses, it is unclear how accurately it captures the interactions in a dynamic situation, and the detailed results are somewhat uncertain. A slightly different potential renders the forces on the neutral atom positive over a larger range of positions, and the range of initial conditions that would result in shuttling would be smaller, implying that the threshold voltage for shuttling depends sensitively on the model for surface-island interactions and on the initial conditions.

The detailed structure of the forces of the middle positions is less important after shuttling is well established. The main forces become the close-range exponential forces of the electrodes and the applied electric field. For the asymmetric shuttle, energy is absorbed by the charged shuttle from the field during half a cycle while during the other half-cycle, after an elastic collision with the electron surface, a neutral shuttle moves nearly freely in the opposite direction. The energy loss during the shuttle-electrode collision cannot exceed the energy absorbed from the field if a stable periodic motion is to be established.

The distribution of positions at which tunneling events take place depends on the transition rates, and the width of the distribution is connected to the spatial derivatives of the rates, *i.e.* on the tunneling lengths. The steeper $1 \rightarrow 0$ gives a more compact distribution as seen in Fig. 7.

The shuttle reaches a stable shuttling motion quickly with a current of $\sim 0.19 \mu\text{A}$ and an amplitude of ~ 11.1

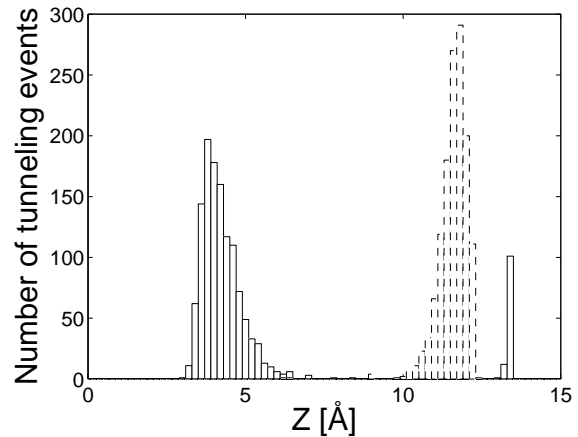


FIG. 7: The statistical distribution of charge transfer locations. The solid and dashed line corresponds to $0 \rightarrow 1$ and $1 \rightarrow 0$ transitions respectively. The quicker growing probability of a $1 \rightarrow 0$ transition compresses the distribution of event locations.

Å, (see Fig. 8). The random character of the transition processes influences the turning points very little. There is, however, a possibility for the system to undergo semi-stable excitations due to randomness of transfer events and the position dependence of the energy spectrum near the right lead (Fig. 9). Very close to the negative (right) lead, there is a possibility of a process in which an electron first tunnels from the electrode to an initially positively charged ($Q = 1$) shuttle that continues to move towards the right lead, followed by tunneling against the bias back into the lead, and finally a new tunneling event after the shuttle has changed its direction of motion. During the time that the charged shuttle spends near the electrode surface after the second tunneling event, it experiences a larger force than a neutral shuttle would, which allows it to absorb more energy from the potential and results in an enhanced shuttling amplitude. The increase in amplitude enhances the possibility for this sequence of three tunneling events to take place also in the next period. The excitation lasts until a transfer without reverse tunneling takes place near the negative lead. For the system we have studied, the amplitude of this excited cycle is about 0.3 \AA larger than that of the simple cycle, and the current level is increased by approximately 20% to $0.23 \mu\text{A}$. The possibility of two stable shuttling amplitudes has recently been discussed by Usmani and co-workers.⁴⁴

IV. DISCUSSION

Both the energy spectra and the (Kohn-Sham) orbitals of small molecules near metal surfaces exhibit a rich structure and vary substantially as a function of the molecule-metal surface separation. The transition rates are largely exponential functions of the tunneling dis-

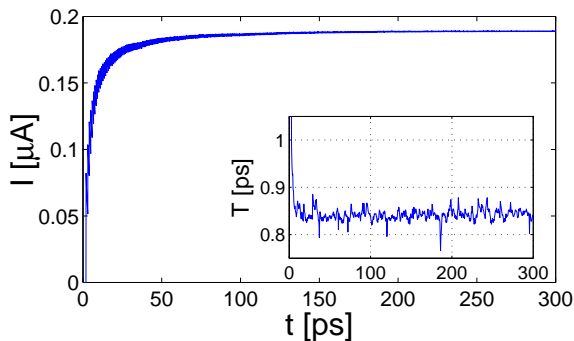


FIG. 8: The average current, n_R/t , where n_R is the number of electrons from the negative lead. Inset: The shuttle period as a function of time. The shuttle quickly reaches a stable motion.

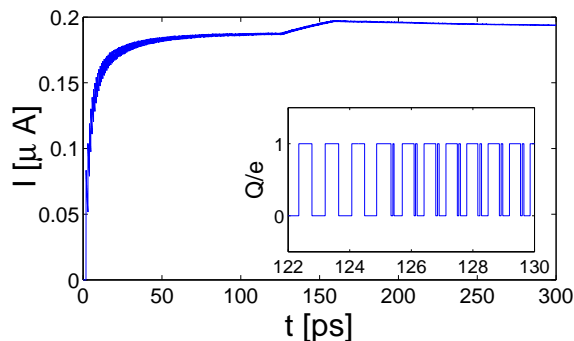


FIG. 9: The average current for a path with system excitation due to back-tunneling close to the negative lead (see inset). The increase of amplitude caused by the larger $Q = 1$ forces enhances the possibility for the tunneling triplet to take place also in the next period. The transition is sharp with an amplitude increase of ~ 0.3 Å and a current of ~ 0.23 μA . The excitation lasts until a period without reverse tunneling takes place.

tance as assumed in phenomenological theories, but the allowed transitions are determined by the energy spectrum, and in particular near the surfaces certain transi-

tions are forbidden by energy considerations. This results in an asymmetry in possible charge states and in asymmetric shuttling where energy is absorbed only during one half cycle of the periodic motion.

The forces in the system are highly sensitive to the description of the electrode-molecule interaction and to the electronic structure of the shuttling object. In the stable shuttling regime the island velocity is large enough for the island to bounce between the repulsion walls, and the details of the forces near the middle of the gap are less important than the balance between dissipation and short range surface forces. The short range forces are hard to describe quantitatively due to the increased importance of many-body effects, deformation of molecular orbitals near surfaces and the details of the dynamic charge transfer processes. However, for large enough speed on impact the mobile molecule may bounce off the surface and establish stable periodic motion.

The shuttle excitations depicted in Fig. 9 are an example of effects that arise due to the details of the energy spectrum of a small system. For a more complicated spectrum and larger bias voltage more phenomena of the same type can be expected; for a slightly different model of shuttle-surface interactions we have even observed that the regular shuttling motion may pass into a more chaotic behavior. Therefore, it is likely that a microscopic picture of both forces and energy levels is paramount for both quantitative and qualitative predictions of molecule-sized shuttles.

Acknowledgments

We acknowledge fruitful discussions with Robert Shekhter, Tomas Nord, and Elsebeth Schröder. This work was supported in part by the European Community FP6 funding through the CANEL project, contract no. FP6-2004-IST-003673. This publication reflects the views of the authors and not necessarily those of the EC. The Community is not liable for any use that may be made of the information contained herein

* chuldt@fy.chalmers.se

¹ M. Roukes, Phys. World **14**, 25 (2001).

² H. G. Craighead, Science **290**, 1532 (2000).

³ L. Y. Gorelik, A. Isacsson, M. V. Voinova, B. Kasemo, R. I. Shekhter, and M. Jonson, Phys. Rev. Lett. **80**, 4526 (1998).

⁴ R. I. Shekhter, Y. Galperin, L. Y. Gorelik, A. Isacsson, and M. Jonson, J. Phys.: Condens. Matter **15**, R441 (2003).

⁵ C. Flindt, T. Novotný, and A.-P. Jauho, Physica E **29**, 411 (2005).

⁶ D. Fedorets, L. Y. Gorelik, R. I. Shekhter, and M. Jonson, Europhys. Lett. **58**, 99 (2002).

⁷ T. Nord, L. Y. Gorelik, R. I. Shekhter, and M. Jonson,

Phys. Rev. B **65**, 165312 (2002).

⁸ S. Braig and K. Flensberg, Phys. Rev. B **70**, 085317 (2004).

⁹ D. Boese and H. Schoeller, Europhys. Lett. **54**, 668 (2001).

¹⁰ K. D. McCarthy, N. Prokof'ev, and M. T. Tuominen, Phys. Rev. B **67**, 245415 (2003).

¹¹ A. Isacsson, L. Y. Gorelik, M. V. Voinova, B. Kasemo, R. I. Shekhter, and M. Jonson, Physica B **255**, 150 (1998).

¹² N. Nishiguchi, Physica E **18**, 247 (2003).

¹³ D. V. Scheible, A. Erbe, and R. H. Blick, New J. Phys. **4**, 86 (2002).

¹⁴ A. Erbe, C. Weiss, W. Zwerger, and R. H. Blick, Phys. Rev. Lett **87**, 096106 (2001).

¹⁵ M. T. Tuominen, R. V. Krotkov, and M. L. Breuer, Phys.

- Rev. Lett. **83**, 3025 (1999).
- ¹⁶ H. Park, J. Park, A. K. L. Lim, E. H. Anderson, A. P. Alivisatos, and P. L. McEuen, *Nature* **407**, 57 (2000).
- ¹⁷ S. Braig and K. Flensberg, *Phys. Rev. B* **68**, 205324 (2003).
- ¹⁸ P. Hohenberg and W. Kohn, *Phys. Rev.* **136**, B864 (1964).
- ¹⁹ W. Kohn and L. J. Sham, *Phys. Rev.* **140**, A1133 (1965).
- ²⁰ E. Runge and E. K. U. Gross, *Phys. Rev. Lett.* **52**, 997 (1984).
- ²¹ A. Kiejna and K. F. Wojciechowski, *Metal Surface Electron Physics* (Pergamon, Oxford, 1996).
- ²² www.fysik.dtu.dk.
- ²³ J. P. Perdew and Y. Wang, *Phys. Rev. B* **45**, 13244 (1992).
- ²⁴ R. O. Jones, P. J. Jennings, and O. Jepsen, *Phys. Rev. B* **29**, 6474 (1984).
- ²⁵ N. D. Lang and W. Kohn, *Phys. Rev. B* **1**, 4555 (1970).
- ²⁶ N. D. Lang and W. Kohn, *Phys. Rev. B* **7**, 3541 (1973).
- ²⁷ P. J. Jennings, R. O. Jones, and M. Weinert, *Phys. Rev. B* **37**, 6113 (1988).
- ²⁸ T. L. Gilbert, *J. Chem. Phys.* **49**, 2640 (1968).
- ²⁹ R. D. Shannon, *Acta Cryst. A* **32**, 751 (1976).
- ³⁰ C. Nordling and J. Österman, *Physics Handbook for Science and Engineering* (Studentlitteratur, Lund, Sweden, 1996).
- ³¹ M. Kunz and T. Armbruster, *Acta Cryst. B* **48**, 609 (1992).
- ³² R. J. Baxter, G. Teobaldi, and F. Zerbetto, *Langmuir* **19**, 7335 (2003).
- ³³ C.-P. E. Varsamis, A. Vegiri, and E. I. Kamitsos, *Condens. Matter Phys.* **4**, 119 (2001).
- ³⁴ S. Adams, *Acta Cryst. B* **57**, 278 (2001).
- ³⁵ J. Bardeen, *Phys. Rev. Lett.* **6**, 57 (1961).
- ³⁶ C. B. Duke, *Tunneling in Solids* (Academic Press, New York, 1969).
- ³⁷ D. Fedorets, L. Y. Gorelik, R. I. Shekhter, and M. Jonson, *Phys. Rev. Lett.* **92**, 166801 (2004).
- ³⁸ A. Y. Smirnov, *Phys. Rev. B* **69**, 155310 (2004).
- ³⁹ N. M. Chtchelkatchev, W. Belzig, and C. Bruder, *Phys. Rev. B* **70**, 193305 (2004).
- ⁴⁰ F. Pistolesi and R. Fazio, *Phys. Rev. Lett.* **94**, 036806 (2005).
- ⁴¹ E. J. Baerends and O. V. Gritsenko, *J. Phys. Chem. A* **101**, 5383 (1997).
- ⁴² D. P. Chong, O. V. Gritsenko, and E. J. Baerends, *J. Chem. Phys.* **116**, 1760 (2002).
- ⁴³ I. O. Kulik and R. I. Shekhter, *Sov. Phys.-JETP* **41**, 308 (1975).
- ⁴⁴ O. Usmani, Y. M. Blanter, and Y. V. Nazarov, *cond-mat/060317* (2006).